

This document is confidential and is proprietary to the American Chemical Society and its authors. Do not copy or disclose without written permission. If you have received this item in error, notify the sender and delete all copies.

**Homogeneous Emission Line Broadening in the Organo Lead
Halide Perovskite $\text{CH}_3\text{NH}_3\text{PbI}_{3-x}\text{Cl}_x$**

Journal:	<i>The Journal of Physical Chemistry Letters</i>
Manuscript ID:	jz-2014-00434p.R1
Manuscript Type:	Letter
Date Submitted by the Author:	n/a
Complete List of Authors:	Wehrenfennig, Christian; University of Oxford, Physics Liu, Mingzhen; University of Oxford, Physics Snaith, Henry; University of Oxford, Physics Johnston, Michael; University of Oxford, Department of Physics Herz, Laura; University of Oxford, Dept. of Physics

SCHOLARONE™
Manuscripts

Homogeneous Emission Line Broadening in the Organo Lead Halide Perovskite $\text{CH}_3\text{NH}_3\text{PbI}_{3-x}\text{Cl}_x$

*Christian Wehrenfennig, Mingzhen Liu, Henry J. Snaith, Michael B. Johnston and Laura M.
Herz**

University of Oxford, Department of Physics, Clarendon Laboratory, Parks Road, Oxford, OX1
3PU, United Kingdom

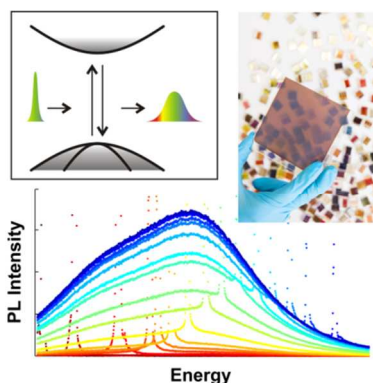
Corresponding Author

*E-mail: l.herz@physics.ox.ac.uk

The organic-inorganic hybrid perovskites methylammonium lead iodide ($\text{CH}_3\text{NH}_3\text{PbI}_3$) and the partially chlorine-substituted mixed halide $\text{CH}_3\text{NH}_3\text{PbI}_{3-x}\text{Cl}_x$ emit strong and broad photoluminescence (PL) around their band-gap energy of about 1.6 eV. However the nature of the radiative decay channels behind the observed emission and in particular the spectral broadening mechanisms are still unclear. Here, we investigate these processes for high-quality vapor-deposited films of $\text{CH}_3\text{NH}_3\text{PbI}_{3-x}\text{Cl}_x$ using time- and excitation-energy dependent photoluminescence spectroscopy. We show that the PL spectrum is homogeneously broadened

with a line width of 103 meV most likely as a consequence of phonon coupling effects. Further analysis reveals that defects or trap states play a minor role in radiative decay channels. In terms of possible lasing applications, the emission spectrum of the perovskite is sufficiently broad to have potential for amplification of light pulses below 100 fs pulse duration.

TOC GRAPHICS



KEYWORDS perovskite, $\text{CH}_3\text{NH}_3\text{PbI}_{3-x}\text{Cl}_x$, Organic-Inorganic, Methylammonium Lead Halide, Time-Resolved Photoluminescence, Femtosecond Lasers, Exciton-Phonon-Coupling

Organometal halide perovskites have recently created a surge of attention following their impressive performance in thin film solar cells.¹⁻⁴ A major advantage of these organic-inorganic hybrid materials is their ability to combine the favourable properties of inorganic semiconductors – especially their high carrier mobilities⁵⁻⁷ – with the flexibility and low-temperature processability of organic materials. Organometal halide perovskites had already been studied to some extent over the past two decades^{5,8-10} when the main applications targeted were thin-film transistors and light-emitting diodes. Research efforts penetrated the whole breadth of the

1
2
3 material class, encompassing fully confined and two-dimensional layered structures that
4 exhibited high tunability of their excitonic properties via the size of the organic cationic
5 molecule.¹¹ More recently, the main focus has been on three-dimensional materials in the classic
6 perovskite configuration ABX_3 , where the cation (A) is a small organic molecule such as
7 methylammonium or formamidinium, B is a metal and X a halogen. In particular, high-quality
8 methylammonium lead iodide ($CH_3NH_3PbI_3$) and the mixed halide obtained by partial
9 substitution with chlorine ($CH_3NH_3PbI_{3-x}Cl_x$) have been successfully used in high efficiency
10 solar cells,^{3,4} where they exhibit favourable optical and electronic properties such as strong
11 optical absorption in the visible and ultraviolet spectrum,² long free charge carrier lifetimes and
12 high carrier mobilities.^{7,12-14} These properties are also highly desirable for many other
13 optoelectronic applications, where organic-inorganic perovskites could once more lead to a step
14 change in feasibility or performance. However, little in-depth knowledge exists to date on what
15 governs the behaviour of the emissive species in these materials.

16
17
18
19
20
21
22
23
24
25
26
27
28
29
30
31
32
33
34
35 In this work we investigate the intense, broad band-edge luminescence from $CH_3NH_3PbI_{3-x}Cl_x$
36 with the intention of unravelling the nature of the emission line broadening and the underlying
37 radiative recombination processes. We focus on thin films fabricated from thermal vapor
38 deposition, which allows for smooth film-formation and high crystalline order making them very
39 suitable for general device applications.⁴ Using photoluminescence spectroscopy with
40 continuously tuneable excitation energy, we scrutinize the broadening mechanism in the mixed
41 halide $CH_3NH_3PbI_{3-x}Cl_x$, which features an emission peak around its band gap energy (1.62 eV)
42 with a full width at half maximum (FWHM) of 103 meV. By scanning the excitation energy
43 across the width of this peak while observing the spectral shape of the PL emission, we establish
44 that the spectral broadening is homogenous. We further acquire time-resolved emission spectra
45
46
47
48
49
50
51
52
53
54
55
56
57
58
59
60

1
2
3 and find that the spectral shape is invariant between 200ps and 200ns after excitation, suggesting
4 an absence of significant disorder-related effects in the emissive species. Based on our
5 observations, we propose strong phonon coupling of charge carriers arising from their polaronic
6 properties as a likely source of the homogeneous broadening. Owing to the uncertainty relation
7 between pulse duration and frequency bandwidth manifested in the natural spectral line width, a
8 broad emission spectrum is one of the primary prerequisites for gain materials in ultrashort
9 (femtosecond) pulsed lasers¹⁵. Here, perovskites could also offer a perspective for electrically
10 pumped designs creating a significant advantage over many well-established fs-laser gain
11 materials which require optical pumping. With the observed spectral width of 103meV, the
12 homogenous gain medium could sustain amplification of light pulses as short as 64fs.
13
14
15
16
17
18
19
20
21
22
23
24
25
26
27
28
29
30
31
32
33
34
35
36
37
38
39
40
41
42
43
44
45
46
47
48
49
50
51
52
53
54
55
56
57
58
59
60

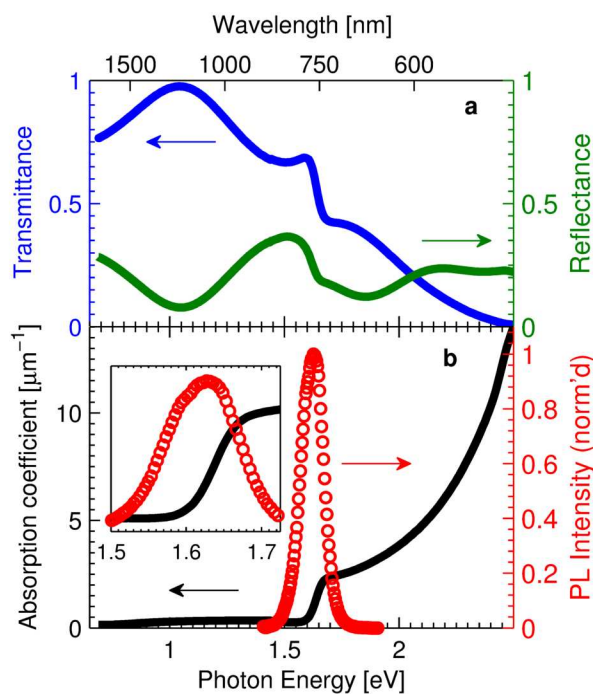


Figure 1: (a) Optical transmittance ($T_{ext} = I_{transmitted}/I_{incident}$, blue) and reflectance spectra ($R = I_{reflected}/I_{incident}$, green) of evaporated films of $\text{CH}_3\text{NH}_3\text{PbI}_{3-x}\text{Cl}_x$. T was determined in specular transmission geometry and R in specular reflection geometry at close to normal (6°) incidence. (b) Black curve: absorption coefficient $\alpha = -1/d \ln(T_{ext}/(1-R))$, calculated from the data in (a) and the film's thickness $d = 330$ nm (black). Red circles: Photoluminescence emission spectrum at 1.96 eV excitation energy ($\lambda = 634$ nm), $6 \mu\text{J}/\text{cm}^2$ fluence and 2 MHz repetition rate. Inset: magnification of the plot in the energy range around the absorption edge and PL emission.

1
2
3
4
5
6
7
8
9
10
11
12
13
14
15
16
17
18
19
20
21
22
23
24
25
26
27
28
29
30
31
32
33
34
35
36
37
38
39
40
41
42
43
44
45
46
47
48
49
50
51
52
53
54
55
56
57
58
59
60

Figure 1a displays the optical transmission and reflection spectra of a vapor-deposited $\text{CH}_3\text{NH}_3\text{PbI}_{3-x}\text{Cl}_x$ film in the NIR/VIS range. The onset of interband absorption can be identified as an edge centred at 1.64 eV, in agreement with previously published data on thin films of solution-processed mixed halide $\text{CH}_3\text{NH}_3\text{PbI}_{3-x}\text{Cl}$ (Refs. 2, 6, 12) and trihalide $\text{CH}_3\text{NH}_3\text{PbI}_3$ (Ref. 16) materials. At photon energies below the steep absorption onset at 1.64 eV, the transmission and reflectance spectra exhibit clear thin-film-interference (Fabry-Perot) effects, which indicates that the film thickness is very uniform and the surface optically flat, preventing any substantial light scattering. From the data in Figure 1a, and the film thickness $d = 330$ nm (determined from SEM cross sectional imaging) we obtain the absorption coefficient shown in Figure 1b together with the PL emission spectrum. Since information on excitonic effects is still emerging and the exact nature of the electronic structure near the band edge is still being explored, extraction of the precise band gap energy is difficult due to the lack of an unambiguous physical description of the absorption onset. A direct semiconductor in accordance with the results of band-structure calculations¹⁷⁻²⁰ ought to exhibit a broad regime for which $\alpha \propto (E - E_g)^{1/2}$ near the absorption onset.²¹ Such a square-root behaviour would at best partly fit the initial steep rise around 1.64 eV leaving the following sharp transition to a flatter regime difficult to account for. On the other hand, absorption enhancements at the band edge caused by resonant exciton creation would provide a plausible explanation for an initially steeper rise of the absorption coefficient.²² Exciton binding energies have been reported for the pure halide $\text{CH}_3\text{NH}_3\text{PbI}_3$ to range from 20 meV (Ref. 23) to 37 meV (Ref. 24), which is sufficiently high for enhancement effects to be observed at room temperature, given that for $T = 297$ K the characteristic thermal energy is $k_B T = 25.6$ meV. We note that reliable clarification of the nature of the absorption onset

may require in-depth theoretical modelling e.g. in conjunction with low-temperature absorption data to allow isolation of individual contributions.

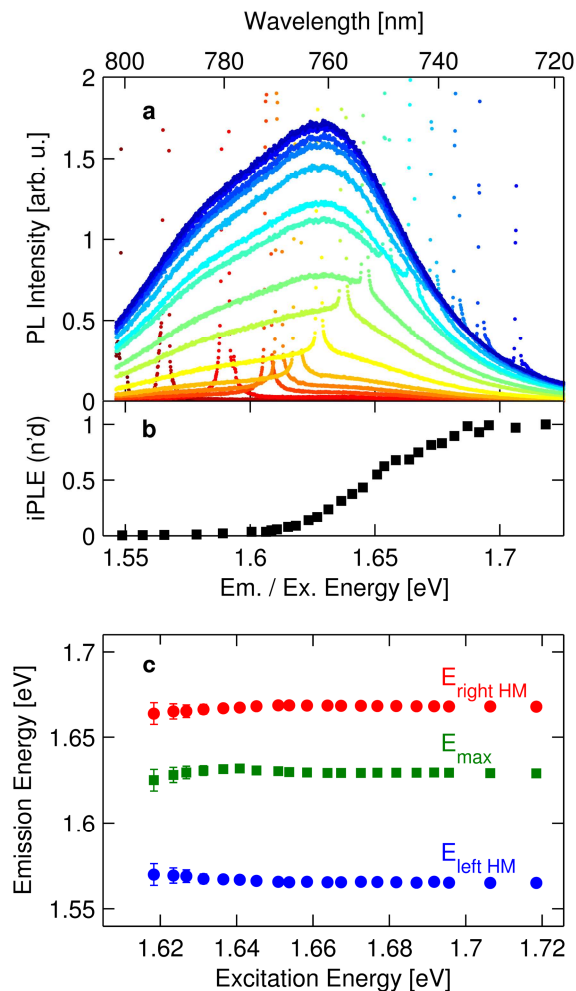


Figure 2: (a) PL emission spectra of evaporated $\text{CH}_3\text{NH}_3\text{PbI}_{3-x}\text{Cl}_x$ films on glass (PL intensity vs. emission energy), taken at excitation energies close to the absorption edge ranging from 1.55 eV (dark red) to 1.73 eV (dark blue). The excitation intensity was held constant at 5 W cm^{-2} . The narrow peaks originate from scattered excitation light and can be used as a visual indicator of the excitation energy. (b) Spectrally integrated PL intensity as a function of excitation energy for evaporated films $\text{CH}_3\text{NH}_3\text{PbI}_{3-x}\text{Cl}_x$ as extracted from the data shown in (a). (c) Energy of the

1
2
3 PL emission maximum extracted from the data shown in (a) plotted against excitation energy
4
5 (green squares). The energies at which the emission reaches half its maximum intensity are
6
7 shown as red and blue circles.
8
9
10
11
12
13
14
15
16
17
18
19
20
21
22
23
24
25
26
27
28
29
30
31
32
33
34
35
36
37
38
39
40
41
42
43
44
45
46
47
48
49
50
51
52
53
54
55
56
57
58
59
60

1
2
3 The photoluminescence emission spectrum of vapor-deposited $\text{CH}_3\text{NH}_3\text{PbI}_{3-x}\text{Cl}_x$ is shown
4 along with the absorption data in Figure 1b. We find that the spectrum has a full-width-at-half-
5 maximum (FWHM) of 103meV. With its centre of mass (1.617 eV) near the low-energy tail of
6 the absorption edge, the PL emission appears to show a slight down-shift in energy with respect
7 to the band gap. The magnitude of any potential shift is however subject to some uncertainty due
8 to the abovementioned ambiguities in the precise location of the band gap energy. Such Stokes
9 shifts are commonly observed in different materials for a variety of reasons including migration
10 of excitations to low-energy sites²⁵ and lattice relaxation (polaronic effects).^{26,27} More
11 remarkable is the apparent presence of additional broadening mechanisms resulting in the
12 emission line width being almost twice as broad as the spectral width of the absorption onset
13 (56meV, determined as the FWHM of the derivative of the absorption edge – see Supporting
14 Information).

15
16
17
18
19
20
21
22
23
24
25
26
27
28
29
30
31
32 To probe the mechanisms that underlie the broadening of the PL emission spectrum, we
33 recorded photoluminescence spectra while scanning the excitation energy through the absorption
34 edge and across the full range of the emission spectrum. For this experiment we operated the
35 Ti:Sapphire pump laser in continuous wave mode to allow spectrally narrow excitation of the
36 sample. A representative subset of the acquired spectra is shown in Figure 2a. Since it is
37 experimentally impossible to fully separate scattered excitation light from the
38 photoluminescence, the spectra also exhibit additional sharp peaks at the corresponding
39 excitation energy. Below, in panel (b) we plot the spectrally integrated PL emission intensity as a
40 function of excitation energy. For this purpose, the PL intensity was normalized for excitation
41 photon flux and the scattered excitation light peaks removed through data interpolation.
42
43
44
45
46
47
48
49
50
51
52
53
54
55
56
57
58
59
60

1
2
3 From the excitation energy dependent PL data we can make the striking observation that across
4 the entire excitation range the emission spectrum has an identical shape. While this result is
5 visually apparent from the spectra shown in Figure 2a, we provide further analysis by extracting
6 the energy of maximum emission and the positions of the left and right half-maxima as a
7 function of excitation energy in Figure 2b (see also normalized spectra in Supporting
8 Information). While the uncertainty increases in the regime of weaker PL emission (as indicated
9 by the error bars), Figure 2b confirms that the emission spectrum of $\text{CH}_3\text{NH}_3\text{PbI}_{3-x}\text{Cl}_x$ is
10 independent of excitation energy across the interband absorption onset. We therefore conclude
11 that the broadening mechanism must be homogeneous, i.e. the emission at every single site is
12 itself equally and fully broadened. If this were not the case, selective excitation within a
13 distribution of inhomogeneous sites would generate charge-pairs only at those sites that are tuned
14 to the particular excitation energy used. As a result, the excitation energy would be site-selective,
15 and the emission spectra shift to reflect the local nature of the sites selected. Such site-selective
16 emission shifts can for example be observed for thin films of disordered polymeric
17 semiconductors exhibiting significant inhomogeneous spectral broadening.²⁵ In contrast, our
18 observation of shape-persistent emission spectra for resonant excitation throughout the emission
19 spectrum of vapor-deposited $\text{CH}_3\text{NH}_3\text{PbI}_{3-x}\text{Cl}_x$ highlights the low degree of disorder present in
20 these thin films.
21
22
23
24
25
26
27
28
29
30
31
32
33
34
35
36
37
38
39
40
41
42
43
44
45
46
47
48
49
50
51
52
53
54
55
56
57
58
59
60

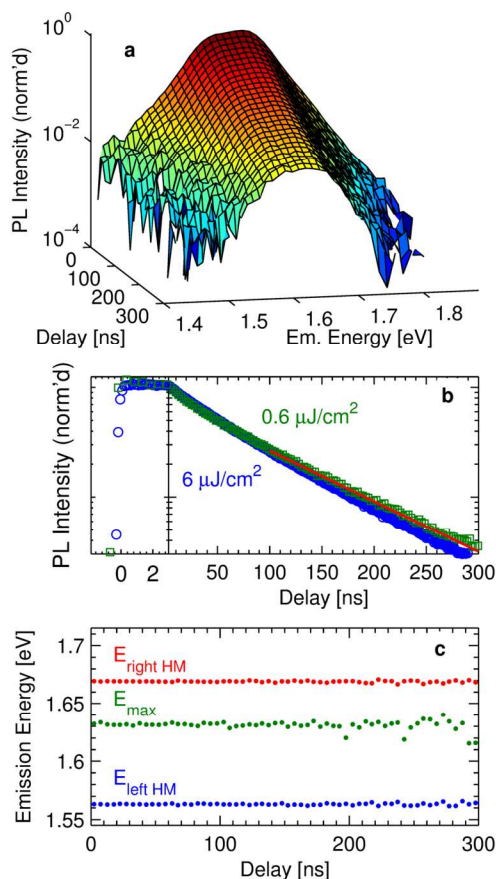


Figure 3: (a) 3D representation of the time-resolved PL emission spectrum of evaporated $\text{CH}_3\text{NH}_3\text{PbI}_{3-x}\text{Cl}_x$ acquired by means of time-correlated single photon counting at various emission energies (Excitation energy: 2.43 eV, fluence: $6 \mu\text{J}/\text{cm}^2$, repetition rate: 2 MHz.) (b) Time-resolved PL emission decay at the spectral maximum for excitation fluences of $6 \mu\text{J}/\text{cm}^2$ and $0.6 \mu\text{J}/\text{cm}^2$ acquired in the same way as the data in (a). Red line: fit of a mono-exponential decay function to the low-fluence data for the time-delay interval from 100 ns to 300 ns. The resulting decay time constant is (94.2 ± 0.9) ns with $\chi^2_{\text{red}} = 1.04$. (c) Photon energy at the emission maximum (green), and the energies at which the emission reaches half its maximum intensity (red and blue) as extracted from the data shown in (a), plotted against the time delay between excitation and emission.

1
2
3 To gain further insights into the dynamics of radiative decay channels in $\text{CH}_3\text{NH}_3\text{PbI}_{3-x}\text{Cl}_x$ and
4 the factors determining the spectral shape of the emission, we recorded time-resolved
5 photoluminescence spectra by means of time-correlated single photon counting (TCSPC). PL
6 decay traces were recorded for a range of regularly spaced emission energies and the spectra at
7 the desired time-delays reconstructed from the data. **Figure 3a** shows the resulting three-
8 dimensional plot of the emission spectra at various times after pulsed excitation at 2.43eV.
9 Visual inspection of these data reveals an essentially time-independent spectral shape of the PL
10 emission (see Supporting Information for normalized spectra). Again we extract the energetic
11 positions of the emission maximum and half-intensity points of each spectrum, to allow for
12 better inspection of potential changes in the spectrum over time (see Figure 3c). This plot clearly
13 confirms that the PL emission spectrum of $\text{CH}_3\text{NH}_3\text{PbI}_{3-x}\text{Cl}_x$ is time-independent for time delays
14 between 200ps and 200ns. Again these results suggest an absence of significant inhomogeneous
15 broadening arising from energetic disorder. For materials incorporating a broad distribution of
16 energetic sites, as for example semiconducting polymer films,^{28,29} porous silicon,³⁰ or heavily
17 doped crystalline GaAs,³¹ pulsed excitation of the material is usually followed by gradual
18 emission shifts towards lower energy with time, resulting from migration to lower-energy sites in
19 the inhomogeneous distribution. The absence of such emission energy shifts with time after
20 excitation in $\text{CH}_3\text{NH}_3\text{PbI}_{3-x}\text{Cl}_x$ films is therefore fully compatible with our prior observation of a
21 predominantly homogeneously broadened emission line width.
22
23
24
25
26
27
28
29
30
31
32
33
34
35
36
37
38
39
40
41
42
43
44
45
46
47

48
49 Figure 3b shows that the PL emission intensity from vapor-deposited $\text{CH}_3\text{NH}_3\text{PbI}_{3-x}\text{Cl}_x$ decays
50 relatively slowly over a few 100 nanoseconds after excitation, in similarity to previous
51 reports^{12,13} for solution-processed films of $\text{CH}_3\text{NH}_3\text{PbI}_{3-x}\text{Cl}_x$. The observed PL transients are
52 almost fully mono-exponential and only exhibit very slightly increasing decay rates for increased
53
54
55
56
57
58
59
60

1
2
3 excitation fluences. As previously reported for solution-processed $\text{CH}_3\text{NH}_3\text{PbI}_{3-x}\text{Cl}_x$ films, such
4 effects arise mainly from the onset of bi-molecular charge recombination, which becomes more
5 and more dominant as the charge-carrier density is increased.⁷ From the PL decay at low
6 excitation fluence ($0.6 \mu\text{J}/\text{cm}^2$) and at longer delays ($>100 \text{ ns}$) after excitation, a mono-molecular
7 decay lifetime of 94 ns can be extracted by fitting a single exponential decay function to the data.
8 We also note that while there is some fluence-dependence of the PL decay rate, the shape of the
9 emission spectra was found to be independent of excitation fluence for values up to at least
10 $20 \mu\text{J}/\text{cm}^2$ (not shown). This observation again suggests an absence of disorder-related effects
11 such as potential saturation of low-energy states in the tail of an inhomogeneously broadened
12 density of states that would induce spectral shifts with increasing excitation fluence.
13
14
15
16
17
18
19
20
21
22
23
24
25
26
27

28 For the discussion of our findings we consider several processes that can potentially cause
29 substantial homogenous PL emission broadening and the observed asymmetry with the spectral
30 broadening of the absorption edge. The simplest origin of homogeneous broadening is given by
31 the natural line width of $\Delta E = \hbar/\tau$ caused by the finite lifetime τ of the excited state.¹⁵ The
32 observed asymmetry between absorption and emission broadening would in this case require at
33 least one additional intermediate state in the recombination process with an extremely short
34 lifetime $\leq 64 \text{ fs}$ (corresponding to $\Delta E = 103 \text{ meV}$), which is six orders of magnitude shorter than
35 the overall decay dynamics we actually observe in time-resolved PL (Figure 3c). In addition,
36 lifetime broadening would have to result in a Lorentzian emission line shape;¹⁵ however the
37 observed spectra (Figure 2a), and in particular the shape of the tails which resemble those of a
38 Gaussian, are not consistent with a Lorentzian distribution function. We therefore conclude that
39 lifetime broadening is not responsible for the dominant contribution to the observed broad
40 emission line width.
41
42
43
44
45
46
47
48
49
50
51
52
53
54
55
56
57
58
59
60

1
2
3
4
5
6
7
8
9
10
11
12
13
14
15
16
17
18
19
20
21
22
23
24
25
26
27
28
29
30
31
32
33
34
35
36
37
38
39
40
41
42
43
44
45
46
47
48
49
50
51
52
53
54
55
56
57
58
59
60

Another possible source of homogeneous broadening lies in the participation of phonons in the radiative recombination process. Figure 2a clearly shows that the PL emission spectra feature a superposition of at least two peaks. It appears that a possible underlying composition could consist of a band-edge emission peak and a number of side bands responsible for the shoulder at about 1.58 eV and the broad tails. PL side-bands are commonly found to arise from phonon creation or annihilation and have been observed in a whole variety of materials, ranging from inorganic semiconductors such as silicon³² and colloidal nanocrystals,³³⁻³⁶ to metal halides³⁷⁻³⁹ and organic (molecular) semiconductors.²⁵ We have recently shown that the low-frequency photoconductivity spectra of solution-processed $\text{CH}_3\text{NH}_3\text{PbI}_{3-x}\text{Cl}_x$ and $\text{CH}_3\text{NH}_3\text{PbI}_3$ films contain the signature of metal halide lattice vibrations.⁷ It therefore seems likely that the emission from such photogenerated charge pairs is also subject to interaction with phonons. Given the large size of the crystallites for these vapour deposited films of $\text{CH}_3\text{NH}_3\text{PbI}_{3-x}\text{Cl}_x$ (extending up to hundreds of nanometers – see Ref 4.) and the absence of time-dependent spectral emission features, the phonon coupling mechanism will most likely arise directly from the intrinsic nature of the bulk material, rather than derive from surface mediated effects. In further support for the presence of such vibrational effects, we show the changes in absorption edge and PL emission spectra for temperature lower than 297K (see Supporting Information). For the absorption edge, a sharpening compatible with a reduction in thermal broadening is observed at 160K. For the PL emission, the high-energy edge sharpens at 160K, as would be expected for reduced phonon absorption at lower temperature. The low-energy edge still shows a side shoulder, in agreement with phonon emission which ought to be largely unaffected by temperature. Hence these results underline the notion of phonon coupling contributing to the emission from this material.

1
2
3 In the picture of electronic band structure, processes involving phonon creation or annihilation
4 simultaneous to the emission of the photon are of particular importance in indirect gap
5 semiconductors where a third particle is needed during electron-hole recombination to accept the
6 momentum difference between conduction band minimum (CBM) and valence band maximum
7 (VBM). Luminescence from indirect semiconductors hence often exhibits a broadened spectrum
8 as e.g. observed in crystalline silicon.³² Band structure calculations have so far postulated a
9 direct band gap for the methylammonium lead halides $\text{CH}_3\text{NH}_3\text{PbI}_3$ (Refs. 17-20),
10 $\text{CH}_3\text{NH}_3\text{PbCl}_3$ (Ref. 19) and $\text{CH}_3\text{NH}_3\text{PbI}_{3-x}\text{Cl}_x$ (Ref. 19). Similar recombination dynamics to
11 those in indirect semiconductors could however also arise from the existence of a second
12 conduction band valley that is only separated from the main (Γ -) valley by a low energy barrier
13 allowing rapid equilibration of their populations. The low bimolecular decay rates and the
14 observation of Auger processes in $\text{CH}_3\text{NH}_3\text{PbI}_{3-x}\text{Cl}_x$ (Refs. 7, 12, 13) suggest that recombination
15 via the direct transition is in some way inhibited, which leaves the possibility for an additional
16 indirect transition to become a dominant recombination pathway. We note however that the
17 likelihood of this scenario to apply in the present case is reduced by the fact that calculations of
18 the electronic band structure of $\text{CH}_3\text{NH}_3\text{PbI}_{3-x}\text{Cl}_x$ have so far not indicated the presence of a
19 second valley.¹⁹

20
21
22 As an alternative concept, the observed broadening may be attributed to polaronic effects,
23 similar to those observed in molecular semiconductors^{40,41} or metal halides.³⁹ Here, the photo-
24 generated electron-hole pair strongly couples to the underlying lattice, which leads to a
25 geometric lattice relaxation around the created charge. As a result, the emission is found to be
26 Stokes-shifted from the absorption edge and likely contains phonon features. For materials with
27 strongly ionic bonding and hence strong exciton-phonon interaction, Coulomb-correlated
28
29
30
31
32
33
34
35
36
37
38
39
40
41
42
43
44
45
46
47
48
49
50
51
52
53
54
55
56
57
58
59
60

1
2
3 electron-hole pairs have therefore also been referred to as “self-trapped excitons”.³⁹ Such
4
5 phenomena have been evoked in alkali halides,⁴² transition metal halides³⁸ and also certain
6
7 perovskites.^{43,44} They are therefore likely to also play a role in the related compounds here. We
8
9 note that for metal halides, the barrier to self-trapping was found to be generally low and the
10
11 process appeared to occur on ultrashort (sub-picosecond) timescales related to the involved
12
13 lattice vibration periods³⁹. We therefore would not necessarily expect any signature of self-
14
15 trapping dynamics in the time-resolved PL spectra shown in Figure 3a, as these were taken with
16
17 much lower time-resolution. Earlier work on alkali halides often revealed significant Stokes
18
19 shifts between absorption and emission.³⁹ For the $\text{CH}_3\text{NH}_3\text{PbI}_{3-x}\text{Cl}_x$ films under investigation
20
21 here, the lack of an unambiguous physical decomposition of the broad absorption and emission
22
23 features prevent the extraction of an exact Stokes shift. However by visual inspection of
24
25 Figure 1b we find that possible values could at most be of the order of 30 meV. This suggests
26
27 that any polaronic effects in this system are comparatively low, in agreement with the high
28
29 charge carrier mobilities⁷ and long diffusion lengths¹²⁻¹⁴ recently reported for solution-processed
30
31 methylammonium lead halide perovskite films. Hence while polaronic effects may be present in
32
33 these materials, they appear to be sufficiently low to still allow excellent charge extraction and
34
35 high open-circuit voltages in planar-heterojunction photovoltaic device architectures.^{4,7,12-14}
36
37
38
39
40
41
42
43

44 Our observation of a strongly homogeneously broadened emission line shape has two
45
46 implications for device applications. First, the absence of spectral shifts resulting e.g. from site-
47
48 selective excitation or excitation migration in these materials suggests that disorder and trapping
49
50 is scarce, at least for the dominant bulk-like emissive species. This finding again highlights the
51
52 suitability of these materials for photovoltaic applications, for which material disorder in systems
53
54 such as organic semiconductors, mesoporous metal oxides and amorphous silicon, has been
55
56
57
58
59
60

1
2
3 shown to correlate with a reduction in photovoltage.⁴⁵ We cannot rule out the presence of
4 disorder or traps near the surfaces of the perovskite, as these contribute little to the overall
5 emission in terms of volume fraction. However, surface states are also highly accessible to
6 passivation treatments^{46,47} that can be more easily applied here than throughout the bulk
7 structure. Second, materials with broad homogeneous emission line shapes fulfill a central
8 requirement for gain media in femtosecond lasers due to the high natural bandwidth of ultrashort
9 pulses (100 meV at 64 fs). Organolead halide perovskites already show many of the required
10 properties for lasing operation, such as strong emission and a sufficiently long-lived upper state.
11 The potential for electrical injection due to the good charge conductivity of the material^{6,7} may
12 create a crucial advantage over existing gain media enabling more compact and efficient laser
13 systems than those relying on optical pumping.
14
15
16
17
18
19
20
21
22
23
24
25
26
27
28
29

30 In conclusion, we have investigated the origin of spectral broadening in the emission of vapor
31 deposited $\text{CH}_3\text{NH}_3\text{PbI}_{3-x}\text{Cl}_x$. By recording PL spectra while continuously tuning the excitation
32 energy across the spectral range of the emission peak we reveal that no observable selective
33 excitation occurs of sub-sites in resonance with the respective energy. We hence establish that
34 the broadening mechanism is homogeneous with an associated width of 103 meV. We
35 furthermore show that the PL emission spectrum does not exhibit a dependence on time after
36 excitation or excitation fluence, suggesting a high degree of order present in the film. The
37 slightly Stokes-shifted and homogeneously broadened PL spectra exhibit features consistent with
38 phonon coupling as the dominant spectral broadening mechanism of the emission from
39 $\text{CH}_3\text{NH}_3\text{PbI}_{3-x}\text{Cl}_x$. Our findings underline the potential of organometal halide perovskites for a
40 wider range of optoelectronic applications beyond photovoltaic energy conversion. In particular,
41 the observed broad homogeneous line width ought to allow amplification of Fourier-transform
42
43
44
45
46
47
48
49
50
51
52
53
54
55
56
57
58
59
60

1
2
3 limited pulses with sub-100fs duration, making these materials interesting for pulsed laser
4
5 operation.
6
7
8
9
10
11
12
13
14
15
16
17
18
19
20
21
22
23
24
25
26
27
28
29
30
31
32
33
34
35
36
37
38
39
40
41
42
43
44
45
46
47
48
49
50
51
52
53
54
55
56
57
58
59
60

Experimental Methods

Sample preparation: Thin films of $\text{CH}_3\text{NH}_3\text{PbI}_{3-x}\text{Cl}_x$ perovskite were deposited by dual source evaporation as described in detail in Ref. 4. Lead chloride (PbCl_2) and methylammonium iodide ($\text{CH}_3\text{NH}_3\text{I}$) were deposited simultaneously onto 1.7 mm thick glass substrates under high vacuum. Before starting the evaporation, the tooling factor (which is a ratio of the material deposited on the sensors to that on the samples) was estimated for each source individually.

Approximately 500 mg of $\text{CH}_3\text{NH}_3\text{I}$ and 100 mg of PbCl_2 were loaded into separate crucibles and the substrates were placed in a substrate holder above the sources. To eliminate volatile impurities in the chamber before coating the substrates with perovskite, the two crucibles were heated above the desired deposition temperatures under high vacuum (10^{-5} mbar) for approximately 5 min. To prepare representative perovskite films, key deposition parameters such as the deposition rates and duration for the two sources were set as previously optimized for best performance of the material in solar cells.⁴ This includes using a $\text{CH}_3\text{NH}_3\text{I}:\text{PbCl}_2$ molar ratio of 4:1 and deposition rates of 5.3 \AA s^{-1} for $\text{CH}_3\text{NH}_3\text{I}$ (crucible temperature around 116°C) and 1 \AA s^{-1} for PbCl_2 (crucible temperature of around 320°C), maintained for approximately 128 min of evaporation. The substrate holder was rotated to ensure uniform coating while the film was deposited on the substrate. Annealing the as-deposited films at 100°C for 45 min in a N_2 -filled glove box enabled full crystallization of the perovskite, darkening the colour and resulting in an apparent growth of crystal features visible in SEM images.⁴ The resulting film thickness is $330 \pm 5 \text{ nm}$.

Photoluminescence Spectroscopy with continuously tuneable excitation is performed using an experimental setup based on a tuneable Ti:Sapphire laser operated in continuous wave mode. A

1
2
3 variable attenuator is used to stabilize the intensity incident on the sample at about 5 W cm^{-2}
4
5 across the full photon energy range. Samples are mounted in a vacuum cell maintaining a
6
7 pressure below 10^{-5} mbar. In this environment the materials is observed to be stable over days
8
9 involving exposure to the excitation light for many hours, with no degradation in PL or visual
10
11 change in film appearance observed for the duration of the measurements. Photoluminescence
12
13 from the sample is collected by a pair of off-axis parabolic mirrors and focussed onto the entry
14
15 slit of a grating monochromator. Polarizers in the excitation and emission beam path ensure that
16
17 only luminescence of perpendicular polarization to the excitation light is detected in order to
18
19 suppress scattered excitation light. Entry slit width and grating constant of the monochromator
20
21 are chosen to achieve a spectral resolution $\Delta\lambda$ better than 0.5 nm. The spectrally resolved PL is
22
23 detected by a nitrogen cooled Si-CCD detector and corrected for spectral response of the
24
25 apparatus by using a tungsten filament lamp of known emissivity spectrum. Unless otherwise
26
27 stated, measurements were taken at room temperature (297K).
28
29
30
31
32
33
34

35 *Time-resolved Photoluminescence* experiments are performed on a PicoQuant FluoTime 300
36
37 fluorescence spectrometer by means of time-correlated single photon counting. A pulsed diode
38
39 laser operating at a photon energy of 1.96 eV (634 nm) excites the sample, which is contained in
40
41 a vacuum chamber at pressures below 10^{-5} mbar, with a repetition rate of 2 MHz. PL is collected
42
43 through a lens and detected at perpendicular polarization with respect to the excitation light. A
44
45 grating monochromator is configured to provide spectral filtering with a resolution $\Delta\lambda$ of about
46
47 2 nm before photons are counted by a hybrid photodetector. A variable attenuator in the emission
48
49 path is used to ensure counting rates are kept below 1 % of the repetition rate to avoid multi-
50
51 photon events. All measurements were taken at room temperature (297K).
52
53
54
55
56
57
58
59
60

1
2
3 *Optical Absorption Spectra* were acquired in a Perkin-Elmer Lambda 1050 UV/VIS/NIR
4
5
6 spectrophotometer with spectral resolution of 2nm.
7
8
9
10
11
12
13
14
15
16
17
18
19
20
21
22
23
24
25
26
27
28
29
30
31
32
33
34
35
36
37
38
39
40
41
42
43
44
45
46
47
48
49
50
51
52
53
54
55
56
57
58
59
60

1
2
3 ASSOCIATED CONTENT
45
6 Supporting Information
7

8
9
10 Derivative of the absorption coefficient. Normalized plots of PL emission spectra. Low-
11
12 temperature PL emission and optical absorption spectra.
13

14
15 This material is available free of charge via the Internet at <http://pubs.acs.org>.
16
17

18
19
20
21 AUTHOR INFORMATION
2223
24 Corresponding Author
25

26
27
28 *Email: l.herz@physics.ox.ac.uk
29

30
31 Notes
32

33
34 The authors declare no competing financial interests.
35
36

37
38 ACKNOWLEDGMENT
39

40
41 The authors gratefully acknowledge funding from the Engineering and Physical Sciences
42
43 Research Council.
44
45
46
47
48
49
50
51
52
53
54
55
56
57
58
59
60

REFERENCES

- (1) Kim, H.-S.; Lee, C.-R.; Im, J.-H.; Lee, K.-B.; Moehl, T.; Marchioro, A.; Moon, S.-J.; Humphry-Baker, R.; Yum, J.-H.; Moser, J. E. et al. Lead Iodide Perovskite Sensitized All-Solid-State Submicron Thin Film Mesoscopic Solar Cell with Efficiency Exceeding 9 %. *Sci. Rep.* **2012**, *2*, 591.
- (2) Lee, M. M.; Teuscher, J.; Miyasaka, T.; Murakami, T. N.; Snaith, H. J. Efficient Hybrid Solar Cells Based on Meso-Superstructured Organometal Halide Perovskites. *Science* **2012**, *338*, 643-647.
- (3) Burschka, J.; Pellet, N.; Moon, S.-J.; Humphry-Baker, R.; Gao, P.; Nazeeruddin, M. K.; Gratzel, M. Sequential Deposition as a Route to High-Performance Perovskite-Sensitized Solar Cells. *Nature* **2013**, *499*, 316-319.
- (4) Liu, M.; Johnston, M. B.; Snaith, H. J. Efficient Planar Heterojunction Perovskite Solar Cells by Vapour Deposition. *Nature* **2013**, *501*, 395-398.
- (5) Mitzi, D. B.; Feild, C. A.; Schlesinger, Z.; Laibowitz, R. B. Transport, Optical, and Magnetic Properties of the Conducting Halide Perovskite $\text{CH}_3\text{NH}_3\text{SnI}_3$. *J. Solid State Chem.* **1995**, *114*, 159-163.
- (6) Stoumpos, C. C.; Malliakas, C. D.; Kanatzidis, M. G. Semiconducting Tin and Lead Iodide Perovskites with Organic Cations: Phase Transitions, High Mobilities, and Near-Infrared Photoluminescent Properties. *Inorg. Chem.* **2013**, *52*, 9019-9038.
- (7) Wehrenfennig, C.; Eperon, G. E.; Johnston, M. B.; Snaith, H. J.; Herz, L. M. High Charge Carrier Mobilities and Lifetimes in Organolead Trihalide Perovskites. *Adv. Mater.* **2014**, *26*, 1584-1589.
- (8) Chondroudis, K.; Mitzi, D. B. Electroluminescence from an Organic-Inorganic Perovskite Incorporating a Quaterthiophene Dye within Lead Halide Perovskite Layers. *Chem. Mater.* **1999**, *11*, 3028-3030.
- (9) Mitzi, D. B.; Chondroudis, K.; Kagan, C. R. Organic-Inorganic Electronics. *IBM J. Res. Dev.* **2001**, *45*, 29-45.
- (10) Mitzi, D. B. Synthesis, Structure, and Properties of Organic-Inorganic Perovskites and Related Materials. In *Progress in Inorganic Chemistry*; John Wiley & Sons: Hoboken, NJ, USA, 2007; Chapter 1, pp 1-121.
- (11) Papavassiliou, G. C.; Koutselas, I. B. Structural, Optical and Related Properties of Some Natural 3-

- 1
2
3 Dimensional and Lower-Dimensional Semiconductor Systems. *Synth. Met.* **1995**, *71*, 1713-1714.
- 4
5
6 (12) Stranks, S. D.; Eperon, G. E.; Grancini, G.; Menelaou, C.; Alcocer, M. J. P.; Leijtens, T.; Herz, L. M.;
7 Petrozza, A.; Snaith, H. J. Electron-Hole Diffusion Lengths Exceeding 1 Micrometer in an Organometal
8 Trihalide Perovskite Absorber. *Science* **2013**, *342*, 341-344.
- 9
10
11 (13) Xing, G.; Mathews, N.; Sun, S.; Lim, S. S.; Lam, Y. M.; Grätzel, M.; Mhaisalkar, S.; Sum, T. C. Long-
12 Range Balanced Electron- and Hole-Transport Lengths in Organic-Inorganic $\text{CH}_3\text{NH}_3\text{PbI}_3$. *Science*
13 **2013**, *342*, 344-347.
- 14
15
16 (14) Gonzalez-Pedro, V.; Juárez-Pérez, E. J.; Arsyad, W. S.; Barea, E. M.; Fabregat-Santiago, F.; Mora-Sero,
17 I.; Bisquert, J. General Working Principles of $\text{CH}_3\text{NH}_3\text{PbX}_3$ Perovskite Solar Cells. *Nano Lett.* **2014**, *14*,
18 888–893.
- 19
20
21 (15) Svelto, O. *Principles of Lasers*; Springer: New York, 2010.
- 22
23
24 (16) Cai, B.; Xing, Y.; Yang, Z.; Zhang, W.-H.; Qiu, J. High Performance Hybrid Solar Cells Sensitized by
25 Organolead Halide Perovskites. *Energy Environ. Sci.* **2013**, *6*, 1480-1485.
- 26
27
28 (17) Koutselas, I. B.; Ducasse, L.; Papavassiliou, G. C. Electronic Properties of Three- and Low-Dimensional
29 Semiconducting Materials with Pb Halide and Sn halide Units. *J. Phys.: Condens. Matter* **1996**, *8*,
30 1217.
- 31
32
33 (18) Umebayashi, T.; Asai, K.; Kondo, T.; Nakao, A. Electronic Structures of Lead Iodide Based Low-
34 Dimensional Crystals. *Phys. Rev. B* **2003**, *67*, 155405.
- 35
36
37 (19) Mosconi, E.; Amat, A.; Nazeeruddin, M. K.; Grätzel, M.; De Angelis, F. First Principles Modeling of
38 Mixed Halide Organometal Perovskites for Photovoltaic Applications. *J. Phys. Chem. C* **2013**, *117*,
39 13902–13913.
- 40
41
42 (20) Even, J.; Pedesseau, L.; Jancu, J.-M.; Katan, C. Importance of Spin–Orbit Coupling in Hybrid
43 Organic/Inorganic Perovskites for Photovoltaic Applications. *J. Phys. Chem. Lett.* **2013**, *4*, 2999-3005.
- 44
45
46 (21) Fox, M. *Optical Properties of Solids*, 2nd ed.; Oxford University Press: New York, 2010.
- 47
48
49 (22) Sturge, M. D. Optical Absorption of Gallium Arsenide between 0.6 and 2.75 eV. *Phys. Rev.* **1962**, *127*,
50 768-773.
- 51
52
53 (23) Sun, S.; Salim, T.; Mathews, N.; Duchamp, M.; Boothroyd, C.; Xing, G.; Sum, T. C.; Lam, Y. M. The
54 Origin of High Efficiency in Low-Temperature Solution-Processable Bilayer Organometal Halide
55 Hybrid Solar Cells. *Energy Environ. Sci.* **2014**, *7*, 339-407.
- 56
57
58 (24) Hirasawa, M.; Ishihara, T.; Goto, T.; Uchida, K.; Miura, N. Magnetoabsorption of the Lowest Exciton
59
60

- 1
2
3
4 in Perovskite-Type Compound (CH₃NH₃)PbI₃. *Physica B* **1994**, *201*, 427-430.
- 5
6 (25) Bäessler, H.; Schweitzer, B. Site-Selective Fluorescence Spectroscopy of Conjugated Polymers and
7 Oligomers. *Acc. of Chem. Res.* **1999**, *32*, 173-182.
- 8
9
10 (26) Pope, M.; Swenberg, C. E. *Electronic Processes in Organic Crystals and Polymers*; Oxford Science:
11 New York, 1999.
- 12
13 (27) Pelant, I.; Valenta, J. *Luminescence Spectroscopy of Semiconductors*; Oxford University Press: New
14 York, 2012.
- 15
16
17 (28) Meskers, S. C. J.; Hübner, J.; Oestreich, M.; Bäessler, H. Dispersive Relaxation Dynamics of
18 Photoexcitations in a Polyfluorene Film Involving Energy Transfer: Experiment and Monte Carlo
19 Simulations. *J. Phys. Chem. B* **2001**, *105*, 9139-9149.
- 20
21
22 (29) Herz, L. M.; Silva, C.; Grimsdale, A. C.; Müllen, K.; Phillips, R. T. Time-Dependent Energy Transfer
23 Rates in a Conjugated Polymer Guest-Host System. *Phys. Rev. B* **2004**, *70*, 165207.
- 24
25
26 (30) Song, L.; El-Sayed, M. A.; Chen, P. C. Spectral Diffusion within the Porous Silicon Emission
27 Wavelength Range on the Nanosecond to Millisecond Time Scale. *J. Appl. Phys.* **1997**, *82*, 836-839.
- 28
29
30 (31) Göbel, E. O.; Graudszus, W. Optical Detection of Multiple-Trapping Relaxation in Disordered
31 Crystalline Semiconductors. *Phys. Rev. Lett.* **1982**, *48*, 1277-1280.
- 32
33
34 (32) Haynes, J. R.; Lax, M.; Flood, W. F. Analysis of Intrinsic Recombination Radiation from Silicon and
35 Germanium. *J. Phys. Chem. Solids* **1959**, *8*, 392-396.
- 36
37
38 (33) Sagar, D. M.; Cooney, R. R.; Sewall, S. L.; Dias, E. A.; Barsan, M. M.; Butler, I. S.; Kambhampati, P. Size
39 Dependent, State-Resolved Studies of Exciton-Phonon Couplings in Strongly Confined Semiconductor
40 Quantum Dots. *Phys. Rev. B* **2008**, *77*, 235321.
- 41
42
43 (34) Kambhampati, P. Unraveling the Structure and Dynamics of Excitons in Semiconductor Quantum
44 Dots. *Acc. Chem. Res.* **2011**, *44*, 1.
- 45
46
47 (35) Mooney, J.; Krause, M. M.; Saari, J. I.; Kambhampati, P. A Microscopic Picture of Surface Charge
48 Trapping in Semiconductor Nanocrystals. *J. Chem. Phys.* **2013**, *138*, 204705.
- 49
50
51 (36) Mooney, J.; Krause, M. M.; Saari, J. I.; Kambhampati, P. Challenge to the Deep-Trap Model of the
52 Surface in Semiconductor Nanocrystals. *Phys. Rev. B* **2013**, *87*, 081201(R).
- 53
54
55 (37) Ikehara, T.; Itoh, T. Dynamical Behavior of the Exciton Polariton in CuCl: Coherent Propagation and
56 Momentum Relaxation. *Phys. Rev. B* **1991**, *44*, 9283-9294.
- 57
58
59
60

- 1
2
3
4 (38) von der Osten, W.; Stolz, H. Localized Exciton States in Silver Halides. *J. Phys. Chem. Solids* **1990**, *51*,
5 765-791.
6
7 (39) Williams, R. T.; Song, K. S. The Self-Trapped Exciton. *J. Phys. Chem. Solids* **1990**, *51*, 679-716.
8
9
10 (40) Heeger, A. J.; Kivelson, S.; Schrieffer, J. R.; Su, W. P. Solitons in Conducting Polymers. *Rev. Mod. Phys.*
11 **1988**, *60*, 781-850.
12
13 (41) Furukawa, M.; Mizuno, K.-i.; Matsui, A.; D. D. V. Rughooputh, S.; C. Walker, W. Time-Resolved
14 Excitonic Luminescence Processes in Poly(phenylenevinylene). *J. Phys. Soc. Jap.* **1989**, *58*, 2976-2987.
15
16 (42) Känzig, W. Electron Spin Resonance of V1-Centers. *Phys. Rev.* **1955**, *99*, 1890-1891.
17
18 (43) Lewis, J. T.; Kolopus, J. L.; Sonder, E.; Abraham, M. M. Reorientation and Motion of the Self-Trapped
19 Hole in KMgF_3 . *Phys. Rev. B* **1973**, *7*, 810-818.
20
21 (44) Tale, I.; Springis, M.; Rogulis, U.; Ogorodnik, V.; Kulis, P.; Tale, V.; Veispals, A.; Fitting, H.-J. Self-
22 Trapped Holes and Recombination Luminescence in LiBaF_3 Crystals. *Radiat. Meas.* **2001**, *33*, 751-754
23
24 (45) Nayak, P. K.; Garcia-Belmonte, G.; Kahn, A.; Bisquert, J.; Cahen, D. Photovoltaic Efficiency Limits and
25 Material Disorder. *Energy Environ. Sci.* **2012**, *5*, 6022-6039.
26
27 (46) Tiwana, P.; Parkinson, P.; Johnston, M. B.; Snaith, H. J.; Herz, L. M. Ultrafast Terahertz Conductivity
28 Dynamics in Mesoporous TiO_2 : Influence of Dye Sensitization and Surface Treatment in Solid-State
29 Dye-Sensitized Solar Cells. *J. Phys. Chem. C* **2010**, *114*, 1365-1371.
30
31 (47) Tiwana, P.; Docampo, P.; Johnston, M. B.; Herz, L. M.; Snaith, H. J. The Origin of an Efficiency
32 Improving "Light Soaking" Effect in SnO_2 Based Solid-State Dye-Sensitized Solar Cells. *Energy*
33 *Environ. Sci.* **2012**, *5*, 9566-9573.
34
35
36
37
38
39
40
41
42
43
44
45
46
47
48
49
50
51
52
53
54
55
56
57
58
59
60